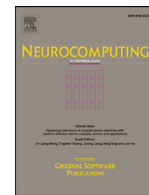




Contents lists available at ScienceDirect



## Neurocomputing

journal homepage: [www.elsevier.com/locate/neucom](http://www.elsevier.com/locate/neucom)

## Haze removal method for natural restoration of images with sky

Yingying Zhu<sup>a,b</sup>, Gaoyang Tang<sup>a</sup>, Xiaoyan Zhang<sup>a,\*</sup>, Jianmin Jiang<sup>a</sup>, Qi Tian<sup>c</sup><sup>a</sup>College of Computer Science and Software Engineering, Shenzhen University, Shenzhen, Guang Dong 518060, PR China<sup>b</sup>Shenzhen Engineering Laboratory for Mobile Internet Application Middleware Technology, Shenzhen University, Shenzhen 518060, PR China<sup>c</sup>Department of Computer Science, The University of Texas at San Antonio, TX 78249, USA

## ARTICLE INFO

## Article history:

Received 10 February 2017

Revised 18 June 2017

Accepted 30 August 2017

Available online xxx

Communicated by Gaofeng MENG

## Keywords:

Haze removal

Luminance model

Dark channel prior

Soft segmentation

## ABSTRACT

Most haze removal methods fail to restore long-shot images naturally, especially for the sky region. To solve this problem, we proposed a Fusion of Luminance and Dark Channel Prior (F-LDCP) method to effectively restore long-shot images with sky. The transmission values estimated based on a luminance model and dark channel prior model are fused together based on a soft segmentation. The transmission estimated from the luminance model mainly contributes to the sky region, while that from the dark channel prior for the foreground region. The airlight also is adjusted to adapt to real light by sky region detection. A user study and objective assessment comparison with a variety of methods on long-shot haze images demonstrate that our method retains visual truth and removes the haze effectively.

© 2017 Published by Elsevier B.V.

## 1. Introduction

In recent years, environmental pollution has led to heavy haze in the Northern China. The images obtained in this region are dusky and fuzzy, which creates problems for working on those images, for example, target detection, recognition and track in aerospace by the devices such as unmanned aerial vehicles (UAV), and taking the aesthetic pictures by mobile phones in daily life. Therefore, the study of image dehazing has its important practical significance. In order to dealing with the haze and redundant color or edges, algorithms have been developed based on the studies on close-range-shot processing. However, in long-range-shots, the far distant area (background) and sky area are difficult to restore. The irradiance in long-range shot is attenuated by much more turbid mediums in atmosphere. There is no standard to estimate its thickness, which results in the restoration of long-shot images being a challenging problem.

The most popular dehazing method is using dark channel prior [1]. The dark channel prior is used to correlate the transmission in a local patch. This method assumes that the intensity in the dark channel is high in the haze region, in contrast, the dark channel value approximates to zero in the haze-free region. However, the truth is that the dark channel value of the sky region without haze is much greater than zero. Therefore, the assumption is not applicable for the sky region. The restored sky region using this

assumption is usually distorted. Some methods have been developed to solve this problem by processing the sky region separately [2–5]. However, it is hard to segment accurately under the heavy haze condition. Another problem in the dark channel prior method [1] is the estimation of the atmospheric light, which is chosen as the color of a pixel from the pixels that are 0.1% of the largest dark channel value. This atmospheric light definition usually causes color shift in the image. Additionally, the atmospheric light is too large and causes the restored images to be dim. Sulami [6] proposed an approach to separately derive the orientation and magnitude of atmospheric light based on their independent assumption. However, there are many cases in which its assumption does not hold and the computational complexity is very high. Tang [7] improved the atmospheric light estimation method by using the median of the 0.1% brightest pixels in the dark channel. This approach can effectively avoid the influence of noise indeed, but it still has the possibility to select pixels from a bright foreground object.

To efficiently and naturally restore the sky region in the dehazing of the haze image, this paper proposes a Fusion of Luminance and Dark Channel Prior (F-LDCP) method. The main steps of the proposed F-LDCP method are medium transmission correction and atmospheric light estimation in the image degradation model. The sky and non-sky regions are processed separately based on a soft segmentation method. By studying images with haze, we observed that the luminance change from foreground to sky is generally coherent with the depth change. Based on this study, the transmission of background and sky regions is proposed to be estimated from the luminance model. The transmission of the

\* Corresponding author.

E-mail address: [xyzhang15@szu.edu.cn](mailto:xyzhang15@szu.edu.cn) (X. Zhang).

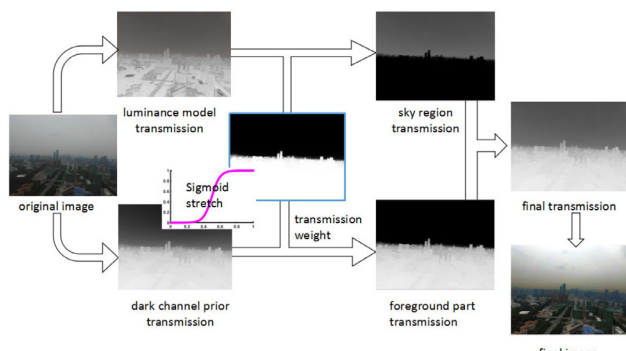


**Fig. 1.** Flow chart of proposed transmission correction algorithm.

foreground region is primarily estimated based on the dark channel prior. The transmissions from the dark channel prior and luminance model are fused together by a transmission weight. The transmission weight is produced by using a Sigmoid model to perform soft segmentation. The framework of the medium transmission correction algorithm is depicted in Fig. 1. According to the physical scattering model, it is reasonable to estimate the atmospheric light from the sky region. Therefore, the atmospheric light is defined as the median of the top 1% brightness pixels in the sky region, which is detected based on the density of edges. The proposed F-LDCP algorithm can significantly increase the visual quality of an atmospherically-degraded image in sense of preserving color distortion and processing the sky area more naturally. Additionally, in the raw transmission refinement, as the traditional Laplace matting method [8] consumes a lot of time and memory, we quote a new method of Fast Guided Filter [9] which is faster than Guided Filter [10] by down-sampling to estimate the dark channel prior transmission map. This saves computation time and makes our F-LDCP method faster than the existing related methods.

## 2. Related work

In recent years, haze removal based on a physical atmospheric scattering model has been very popular. Since Nayer and Narasimhan [11,12] described and deduced the atmospheric scattering model in 1999, many single image haze removal algorithms have been proposed based on their model. Tan [13] proposed to estimate airlight and compute the direct attenuation by maximizing the contrast of the image based on Markov Random Field for haze removal. However, this method resulted in oversaturation and heavy color shift. In the model proposed by Fattal [14], it was assumed that the surface shading was a constant and it was divided into two directions to estimate the color of the haze using a physical model. This method failed in heavy haze and low contrast regions. Kopf [15] removed haze by estimating the transmission based on real depth captured by georeferenced 3D terrain models. Though it was effective, increased costs were necessary to capture real depth. To process dehazing fast, Tarel [16] proposed to use an atmospheric veil which was similar to dark channel matting with a median filter. However, many parameters need to be adjusted to obtain acceptable results. A prior probability of scene radiance dehazing model was developed [17]. It enabled the integration of structural constraints as statistical priors on both the depth and albedo. Meng [18] proposed to estimate an optimized transmission map through combining contextual regularized weighted L1-norm and the inherent boundary constraint for image dehazing. Except for Kopf's method [15], the other methods are inefficient for the sky treatment effect. The dark channel prior method proposed by He et al. [1] is a breakthrough in the dehazed area. However, it

still has limitations on the processing of the sky region and color distortion after haze removal. Li [19] modified atmospheric light estimation to improve color distortion. It is hard to confirm that the color modification is in line with the true color of the scene.

In order to retain the natural appearance of image after dehazeing, some works applied a luminance prior method for haze removal. The authors in [20] reported that the intensity value vary sharply along with the change of the haze concentration. The residual error between intensity and haze concentration was close to zero. Therefore, the linearly transformed luminance was used to simulate the depth for haze removal of the entire image. A linear learner model (Color Attenuation Prior [21]) was created by using the difference between the brightness and the saturation to estimate scene depth for haze removal. The results of the two methods were natural, but the haze removal effect in foreground was not ideal.

Some methods were proposed to produce natural sky in dehaze images by segmenting the sky and non-sky regions and processing them separately. The work in [2] segmented the sky and non-sky regions based on gradient of intensity. A constant threshold was used to segment sky and non-sky regions based on transmission map and intensity in [3]. Gaussian Mixture Model (GMM) was to cluster the depth map to sky and non-sky regions in [4]. Yoon [5] proposed a context-adaptive superpixel segmentation method to segment image into labels include sky and ground. In images with heavy haze, the sky and far away background are connected together. It is hard to get the accurate boundary line between sky and non-sky regions in heavy haze image by using these methods above [2–5]. Non-natural artificial lines may be created in the dehazed result by using the inaccurate segmentation results. In [22], the authors reported a new refine method by segmenting dark channel value patch with neighboring pixels instead of soft-matting method or guided-filtering method.

Along with the increasing population of deep learning, learning framework for dehazing was proposed by Tang [7] and a supervised learning method by learning the parameters of the dehaze model was proposed by Zhu [21]. A holistic transmission map was predicted by using a multi-scale deep network in [23]. Cai [24] proposed a DehazeNet model adopting Convolutional Neural Networks (CNN). The CNN layers were specially designed to embody the established priors in image dehazing. The results were natural, but were dim. The main reason was that the atmospheric light was estimated by simply picking out the largest intensity value in the image.

## 3. Proposed F-LDCP method

### 3.1. Image degradation model

In computer vision and image processing, the widely used image degradation model is described as [25]:

$$I(x) = J(x)t(x) + A(1 - t(x)) \quad (1)$$

where  $I$  is the observed intensity with haze,  $J$  is the real scene to be recovered,  $A$  is the global atmospheric light, and  $t$  is the medium transmission expressing the light that survives the path between the observer and a surface point in the scene. Haze removal is to restore the haze-free image  $J$  from original haze image  $I$ .

The turbidity of the atmosphere raises with the increasing distance of an object and atmospheric degradation factors. Since the transmission determines the reaching proportion of the light which is reflected from the object to the camera, light traveling a longer distance is more attenuated [13]. Therefore, the transmission can be expressed as:

$$t(x) = e^{-\beta d(x)} \quad (2)$$

where  $d$  is the depth of scene, and  $\beta$  is the scattering coefficient, which depends on aerosol type, size and concentration, light wavelength, polarization state, etc.

### 3.2. Dark channel prior transmission

The dark channel prior is based on a type of statistic of dark channel values of outdoor haze-free images without sky. In most of the haze free image patches, at least one color channel has very low intensity at some pixels. Since natural outdoor images are usually full of shadows or colorful objects, these objects with low dark channel values are really dark, i.e. the dark channel of the haze-free image  $x$  tends to be zero, it is defined as:

$$J^{dark}(x) = \min_{y \in \Omega(x)} \left( \min_{c \in \{r,g,b\}} J^c(y) \right) \rightarrow 0 \quad (3)$$

where  $J^c$  is one color channel value of  $J$  and  $\Omega(x)$  is a local patch which centered at  $x$ . According to statistics, the transmission after being normalized and calculated by dark channel on the both sides can be estimated by:

$$\tilde{t}_d(x) = 1 - \omega \min_{y \in \Omega(x)} \left( \min_{c \in \{r,g,b\}} \frac{I^c(y)}{A^c} \right) \quad (4)$$

where  $\omega(0 \leq \omega \leq 1)$  is a coefficient describing the degree of the de-hazing to present depth.

To get the speedy algorithm as well as to ensure the quality, the dark channel transmission  $\tilde{t}_d$  is refined by Fast Guided Filter [9] to remove artifact blocks and halos. The Fast Guided Filter is faster than Guided Filter [10] and has a computational complexity of  $O(N/s^2)$ , where  $s$  is a subsampling ratio. The estimated raw transmission  $\tilde{t}_d$  in Eq. (4) and the original hazy color image  $I$  are subsampled by  $s$ . The transmission image is corrected by the weighted average of the guided filter as:

$$t_d(\bar{x}) = \sum_{\bar{y}} W_{\bar{x}\bar{y}}(I^c(\bar{x})) \tilde{t}_d(\bar{y}) \quad (5)$$

where  $\bar{x}$  and  $\bar{y}$  are the pixel coordinates after subsampling. The weighted filter kernel  $W_{\bar{x}\bar{y}}$  is given as:

$$W_{\bar{x}\bar{y}}(I^c(\bar{x})) = \frac{1}{|\omega|^2} \sum_{k:(\bar{x},\bar{y}) \in \omega_k} \left( 1 + \frac{(I^c(\bar{x}) - \mu_k)(I^c(\bar{y}) - \mu_k)}{\sigma_k^2 + \varepsilon} \right) \quad (6)$$

where  $\omega_k$  is a window centered around  $k$ ,  $|\omega|$  is the number of pixels in  $\omega_k$ ,  $\varepsilon$  is a regularization parameter,  $\mu_k$  is the mean and  $\sigma_k$  is the variance of pixel values in  $\omega_k$ .

### 3.3. Luminance model

In the original dark channel prior method, it is assumed that the dark channel values of the haze-free image equal zero after being normalized by atmosphere light. This assumption is not applicable to the sky region of images. Several haze free images with clear sky under dark channels are shown in Fig. 2. The dark channel values in the sky region are much larger than zero. This is the reason why the recovered color inevitably deviates from the original scene and looks unnatural in the sky region after using the original dark channel prior method. Therefore, the dark channel prior method is unsuitable to deal with sky region. In the same way, when the color of objects is inherently similar to the atmospheric light and no shadow is casting on them, the dark channel prior is invalid (See the road in Fig. 2(d)). Based on the image degradation model in Eq. (1), the actual transmission is:

$$t_{actual}(x) = \frac{1 - I_c(x)/A_c}{1 - J_c(x)/A_c} \quad (7)$$

According to the assumption in Eq. (3), the denominator in Eq. (7) should be set as one for the estimated transmission value. In reality, the estimated transmission is less than its real value in the sky region. According to the above analysis, the effectiveness of haze removal will be decreased in sky region because it demands larger transmission value to preserve the naturalness, especially when the existence of natural texture such as clouds in the sky region. The depth of the sky region is indefinite. It is impossible to capture the real depth of the sky. By studying images with haze, we observe that the distribution of the luminance (from HSL color space) in an image with haze is generally coherent with the change of depth. The luminance of the sky region is much greater than the foreground (see the average luminance of 5000 images with haze in Fig. 3).

Therefore, we proposed to use the luminance to simulate scene depth. The estimated transmission based on the luminance could be expressed as:

$$t_L(x) = e^{-\beta \tilde{L}(x)} \quad (8)$$

where  $t_L$  is the transmission estimated from luminance.  $\tilde{L}$  is the modified luminance,  $\beta$  is the scattering coefficient. The details of the scattering depend on what types of particles are in the atmosphere. Some models have been developed to simulate the atmosphere scattering, e.g., Rayleigh scattering model, Mie scattering model [26] and Henyey and Greenstein phase function [27]. Among them, the most commonly used models are the Rayleigh and Mie scattering theory [26]. Rayleigh's law of atmospheric scattering provides the relationship between the scattering coefficient  $\beta$  and the wavelength  $\lambda$  [11], which is defined as:

$$\beta(\lambda) \propto \frac{1}{\lambda^\gamma} \quad 0 \leq \gamma \leq 4 \quad (9)$$

where  $\beta$  depends on the size of particles distributed in the atmosphere. In the hazy atmosphere, the size of haze particles is larger than the wavelength of the light, and  $\gamma$  takes its minimum value, such as  $\gamma \approx 0$ . Meanwhile,  $\beta$  is closed to a constant and is less dependent on the wavelength of light. Mie scattering model [11,26] is applicable to this condition. The scattering coefficient is determined by the amount of haze, object distance and camera angle. A camera angle of  $60^\circ$  is sufficient to capture images with sky. Therefore, the scattering coefficients corresponding to a camera angle of  $60^\circ$  in the Mie scattering model [5] are used in our work, which are defined as:

$$\beta = \begin{cases} 0.3324, \lambda = 700 \mu\text{m}(\text{red}) \\ 0.3433, \lambda = 520 \mu\text{m}(\text{green}) \\ 0.3502, \lambda = 440 \mu\text{m}(\text{blue}) \end{cases} \quad (10)$$

In order to simulate the real depth, the luminance is stretched by a parameter as follows:

$$\tilde{L}(x) = \frac{\tau}{l^*} l(x) \quad (11)$$

where  $l$  is the luminance of the input image.  $\tau$  describes the real depth range.  $l^*$  is range of current luminance, which is set as the 95% percentile value of the luminance in the experiment. The stretch of luminance into real depth range will results in that the distribution of luminance transmission is in similar value range of dark channel prior transmission. In other word, the luminance transmission and dark channel prior transmission are aligned after stretching luminance by Eq. (11). The depth range  $\tau$  is determined based on an optimization procedure which is described in Section 4.4.

### 3.4. Fusion of the two transmission models

Using the estimated transmission under the luminance model may not perform well for the restoration of the foreground region



**Fig. 2.** Top: example haze-free images. Bottom: corresponding dark channel maps.

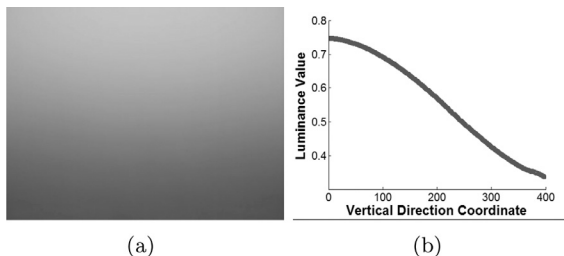


**Fig. 3.** Statistics of luminance. (a) The average luminance map of 5000 images with haze in resolution of  $400 \times 600$ . It is calculated by resizing all the images to the same size ( $400 \times 600$ ) and then calculating the pixel-wise average of the luminance image. (b) The average values of respectively 400 rows for the average lightness image in (a). It describes the average luminance change from sky to foreground. The luminance is calculated in HSL color space.

(creates color shift in foreground region, ref to the enlarged window in Fig. 4(g)). This is because the estimated depth is more likely inaccurate due to objects shading and occlusion in the foreground. While the dark channel prior method aims at non-sky images and performs well for foreground region dehazing. Therefore, we propose to use dark channel prior to estimate the transmission of the foreground region, and use the luminance model to process the sky region, i.e., we propose a fusion model. The fusion of the two transmissions is expressed as:

$$T(x) = C(x, o_s)t_L(x) + C(x, o_f)t_d(x) \quad (12)$$

where  $T$  is the final transmission after modification,  $t_L$  is the transmission estimated from luminance,  $t_d$  is the transmission estimated from dark channel prior which is refined by Fast Guided Filter [9], and  $C(x, o_s)$  and  $C(x, o_f)$  represent the likelihood of the pixel  $x$  belonging to two different classification (sky or foreground). And we defined:

$$C(x, o_f) = 1 - C(x, o_s) \quad (13)$$

For accurate  $C(\cdot)$ , we first tested hard segmentation methods based on edge density [28,29]. Even though sensitive enough to identify the sky region according to edge density differences, it is still hard to accurately detect the boundary between the sky and non-sky regions in heavy haze images which will cause the abrupt effectiveness between the two parts after dehazing. In order to avoid above mentioned problem, we propose a soft segmentation method based on obtaining gradually-changed weight from transmission map of dark channel prior. The dark channel prior transmission value in the sky region is uniformly low. On the contrary, the transmission value in the foreground region is uniformly high. Therefore, the transmission values in the sky and foreground regions can be used to represent the weight of pixel belonging to the sky and foreground respectively. In addition, the transmission weight already carries the outline of objects so we could get the good edge features. Based on this observation, the dark channel

prior transmission perfectly meets the requirements for creating the transmission weight map.

### 3.5. Sigmoid function stretch

Although the source of the transmission weight map is confirmed, the intervals of the values are unsatisfactory. A Sigmoid model is used to generate the transmission weight with a smoothing transition from the foreground region to the sky region, which is expressed as:

$$w(x) = \frac{1}{1 + e^{-\theta_1(t_d(x) - \theta_2)}} \quad (14)$$

where  $\theta_1$  is the parameter that affects the degree of inclination of the curve.  $\theta_2$  is the center of the horizontal coordinate and is set according to the range of image transmission value.

The parameters  $\theta_1$ ,  $\theta_2$  are determined based on two control points  $(t_{ds}, S(g_s))$ ,  $(t_{df}, S(g_f))$ , where  $S$  is the standard Sigmoid function (red curve in Fig. 5).  $g_s$  and  $g_f$  are two points in the standard Sigmoid curve  $S$  which their dependent value close to 0 and 1, respectively.  $t_{ds}$  and  $t_{df}$  are the transmission values of the sky and foreground regions respectively. By substituting the two control points in Eq. (14), it results in the linear equation:

$$\begin{cases} g_s = \theta_1 t_{ds} - \theta_1 \theta_2 \\ g_f = \theta_1 t_{df} - \theta_1 \theta_2 \end{cases} \quad (15)$$

Therefore, these parameters  $\theta_1$ ,  $\theta_2$  can be solved as:

$$\theta_1 = \frac{g_f - g_s}{t_{df} - t_{ds}} \quad (16)$$

$$\theta_2 = \frac{g_f - t_{df}\theta_1}{\theta_1} \quad (17)$$

$g_s$  and  $g_f$  are set as a predefined constant value which have  $S(g_s)$  and  $S(g_f)$  close to 0 and 1, respectively. In order to stretch the foreground region to have a weight value of 1 and stretch the sky region to have a weight value of 0,  $t_{ds}$  and  $t_{df}$  are defined as the average transmission values in sky region and foreground region respectively. The curve of the Sigmoid transform could be adaptively defined based on the dark channel prior transmission map. Different haze images have different transmission weight curves (Sigmoid transform curve) (see Fig. 6).

As for the parameters of  $g_s$  and  $g_f$ , we had tested different values. The transmission weight curves generated by using different  $g_s$  and  $g_f$  values of an example image are shown in Fig. 7. We find that the large values of  $|g|$  ( $|g_s|$  and  $|g_f|$ ) could not produce distinct difference from that using  $|g| = 6$ . The dehazed results by using the larger values have no obvious difference from that using  $|g| = 6$  too. The dehazed results by using  $|g|$  smaller than 6 have relatively poor foreground clarity. Therefore, we select  $|g|$  equals to 6 in our experimental setting.

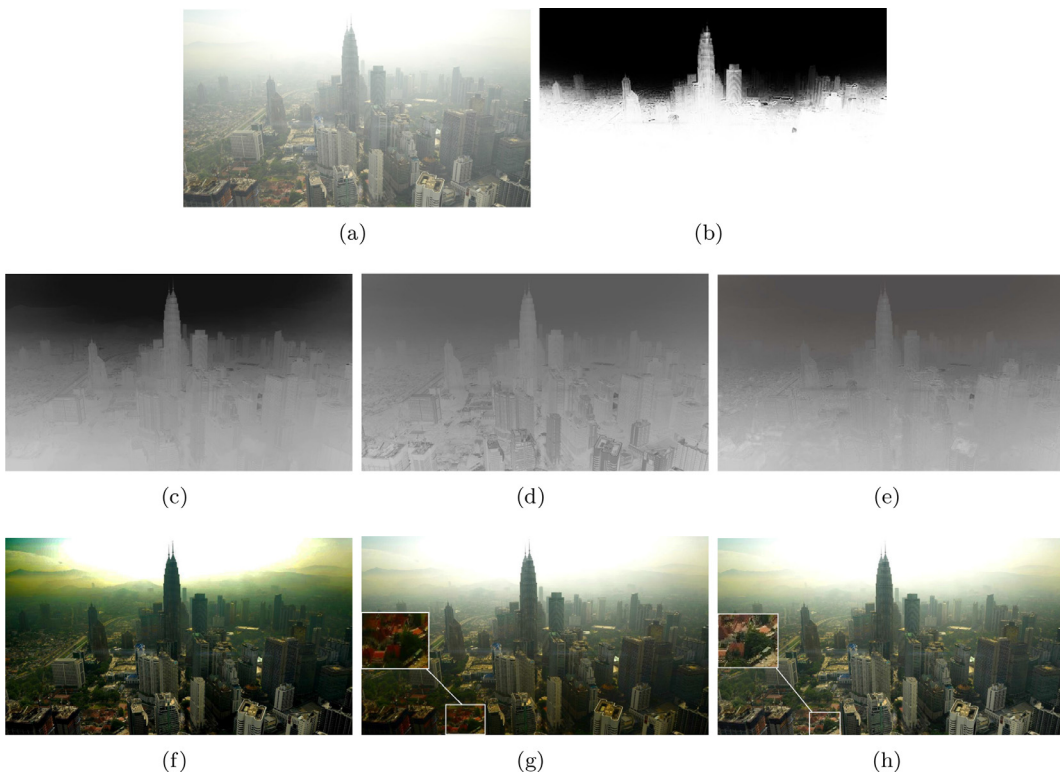


**Fig. 4.** (a) Original image. (c) Dark channel prior transmission. (d) Luminance transmission. (e) Transmission after fusing (c) and (d) using the transmission weight in (b). (f-h) Dehazed images derived by corresponding transmissions in (c)-(e).

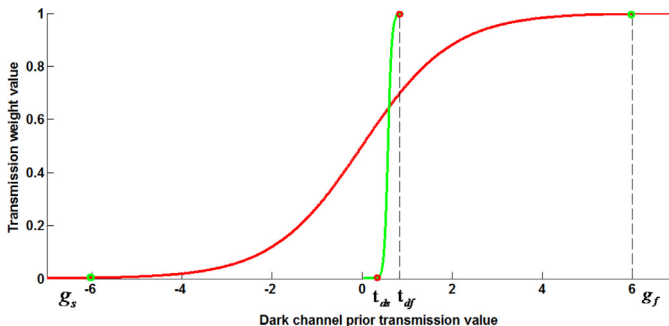


**Fig. 5.** Sigmoid curve and transmission weight curve. The green curve is Sigmoid curve after stretching (transmission weight curve). The red curve is the standard Sigmoid curve. (For interpretation of the references to color in this figure legend, the reader is referred to the web version of this article.)

As shown in Fig. 6, the weight of the sky region approximates to 0, and it approximates to 1 in the foreground region. Comparing to hard segmentation of the sky and foreground regions, our soft segmentation based on the Sigmoid model saves a lot of computation time. Our result in Fig. 6(b) also has good effect in both foreground and sky visually using our transmission map.

### 3.6. Atmospheric light estimation and final recovery

The failure of the dark channel prior method is also due to the atmospheric light estimation. The 0.1% brightest pixels in the dark channel are selected. Among these pixels, the pixel with highest intensity in the input Image is selected as the atmospheric light. However, the largest dark channel value is normally in the foreground like a white building or car in a high brightness value. The atmospheric light probably is incorrectly estimated using this way. Nayar [11] deduced that the airlight is the radiance in the

horizontal direction when the scene depth is infinitely large. According to the physical phenomenon, the atmospheric light should be chosen from the sky region. This is because the sky region is the furthest region and the most haze-opaque region.

Our proposed method detects the sky region and picks out pixels with the relative maximum dark channel value in the sky region to estimate the atmospheric light. With the effect of haze, the sky region in the captured image almost has no texture. So we use the edge detection with the Canny operator to detect the edge, and define sky area through judging density of edges. The heavy haze sky region has less edges and is relatively homogeneous. We convoluted the entire edge map with a small window, and set a threshold to distinguish whether the area is the sky or not. Then the largest connected region with low edge density is detected as the sky region. The median value of the 1% brightest pixel values in the sky region is defined as the atmospheric light  $A$ . The reason for selecting the median value instead of the largest value is that it is robust to noise. Thus, it decreases the effect of noise and results in natural color restoration.

Finally, we can recover the scene radiance according to Eq. (1), the final scene radiance  $J(x)$  is recovered by:

$$J(x) = \frac{I_c(x) - A_c}{\max(T(x), t_0)} + A_c \quad (18)$$

where a low bound  $t_0$  is given to preserve a small amount of haze in very dense haze regions.

## 4. Experimental results

In this section, the effectiveness of our proposed F-LDCP approach is evaluated in several experimental analysis. They are comparison with luminance prior methods, evaluation of soft segmentation, atmospheric light estimation, the parameter selection, and comparison with six stat-of-the-art haze removal methods through user study, time cost and objective assessment.

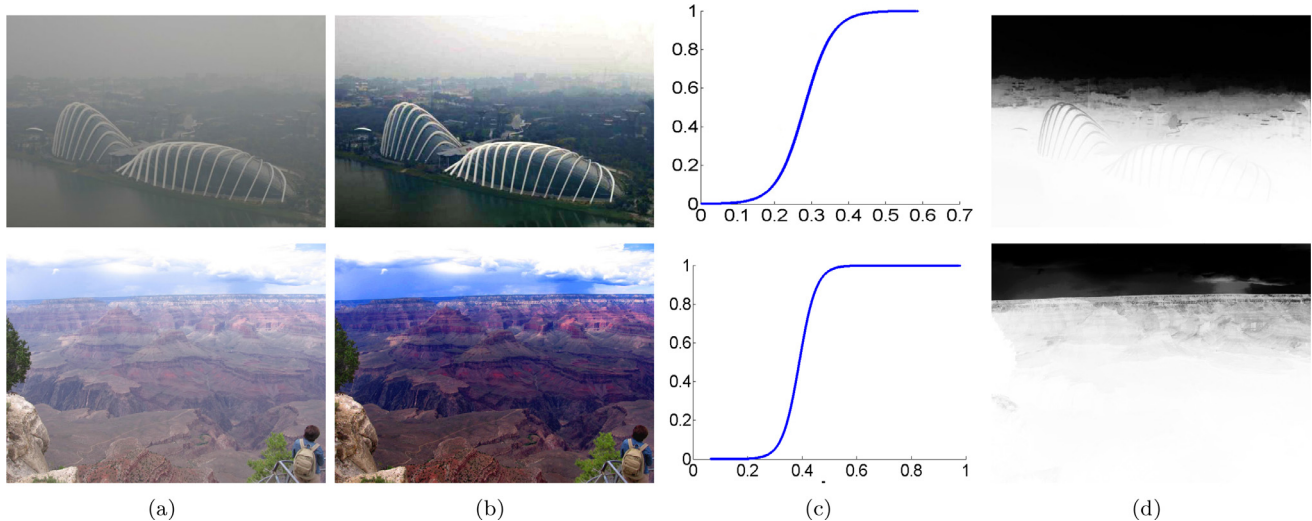


**Fig. 6.** The effect of Sigmoid curve in different images and transmission weight maps. (a) Input haze image (b) Dehazed image by F-LDCP method. (c) Sigmoid curve adaptively generated. (d) Transmission weight map.

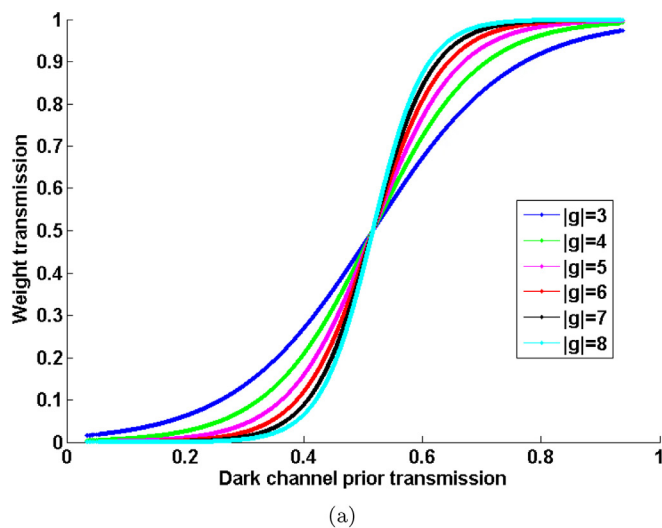


**Fig. 7.** The results generated by using different  $g$  ( $g_s$  and  $g_f$ ) values. (a) Transmission weight curve by different  $|g|$  stretching (b) Original image (c–f) The parameter set in different values of  $|g| = 3, 4, 5, 6, 7, 8$ .

#### 4.1. Luminance prior comparison

Our method is a fusion of luminance prior and dark channel prior for haze removal. Some methods propose to use the luminance prior only to conduct haze removal [20,21]. The linearly transformed luminance is used to simulate the depth for haze removal of the entire image in [20]. The depth of the scene is simulated by a linearly transformed difference between the brightness and the saturation in [21]. In order to show the advantage of our method, the dehazed results of these two methods are compared with our results in Fig. 8. These two methods could generate dehazed results with natural sky. However, the dehazing effect in the foreground does not perform well. The foreground objects

may have distinct luminance even though they may in the same depth. We can see the results by these two methods retain some haze in the foreground region (Fig. 8(b) and Fig. 8(c)). Dark channel prior method has good dehazed effect in the foreground, however, the sky regions have distortions. We use linearly transformed luminance to simulate depth in the sky region only while the foreground depth is determined by using dark channel prior. The results by our method are the best.

#### 4.2. Evaluation of soft segmentation

Some segmentation results using our method are shown in Fig. 9. We also compare our segmentation results with those

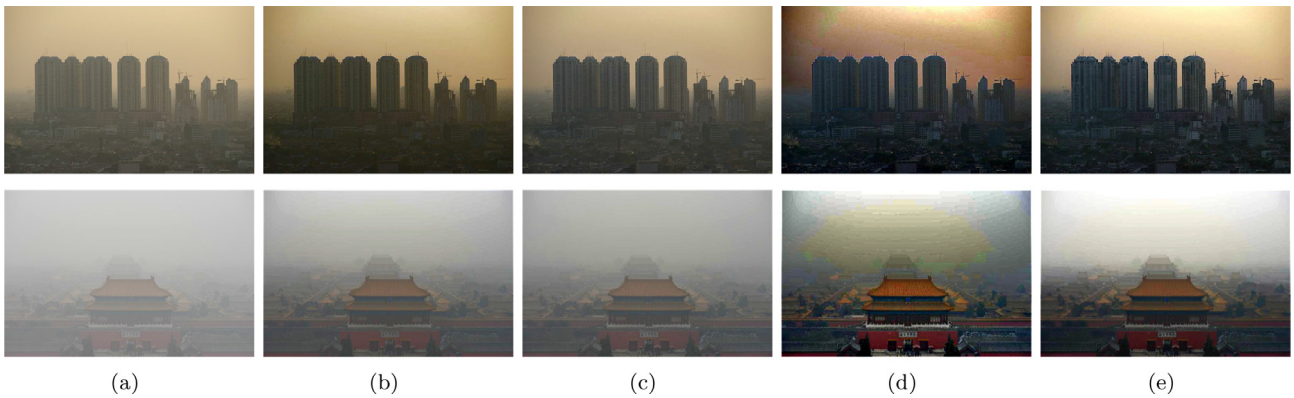


**Fig. 8.** The comparison of dehazed results with luminance prior methods. (a) Original images (b) Results by Cai et al. [20]. (c) Results by Zhu et al. [21]. (d) Results by Dark channel prior [1] (e) Our results.

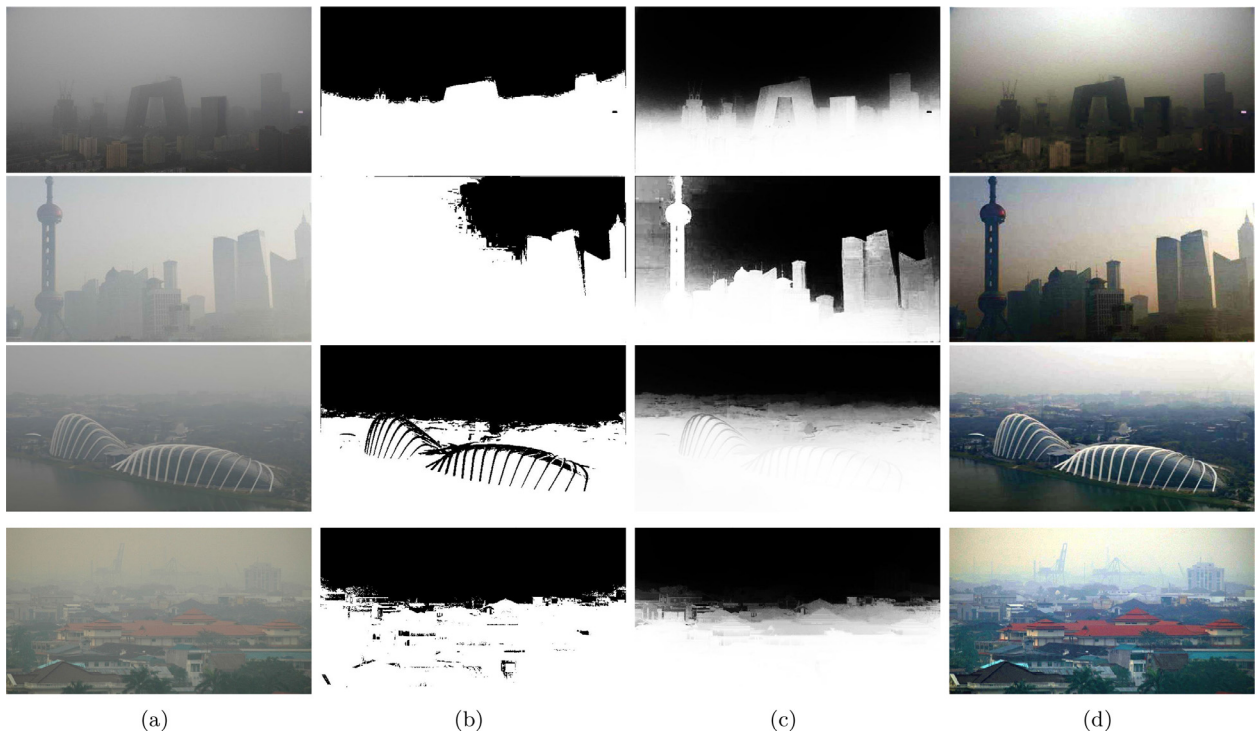


**Fig. 9.** The comparison of segmentation method with the proposed method. (a) Input image. (b) GMM segmentation. (c) Our soft segmentation. (d) Dehazed image by our method.

generated by a Gaussian Mixture Model (GMM) method [4]. GMM is utilized to cluster the depth map to the sky and non-sky regions. In images with heavy haze, the sky and far away background are connected together. We can see that the GMM method could not accurately find the boundary line between sky and the profile of the objects in images with heavy haze (see results in the first two rows in Fig. 9(b)). However, our soft segmentation results have natural transition from foreground to sky while retain the outlines of objects better than GMM segmentation method in images with heavy haze. It results in natural transition from foreground to sky in the dehazed results (Fig. 9(d)). Our soft segmentation method could produce dehazed results without artifacts (see Fig. 9(d)) that may be created by inaccurate hard segmentation.

#### 4.3. Atmospheric light estimation

The effect of our atmospheric light estimation on the dehazed results is compared with the estimation used in the original dark

channel prior method [1]. A comparison is shown in Fig. 10. The sky region segmentation results are feasible in Fig. 10(b). The hollow rings in magnified area in Fig. 10(a) are the pixels of the atmospheric light chosen in original image. The atmospheric light of the dark channel prior method is shown in blue ring, and that of our method is shown in red ring. The atmospheric light of the dark channel prior method is chosen from the bright foreground object, which is unreasonable. We can see that the results produced by the original dark channel prior method has the color shift because of the error associated with the atmospheric light selection (see Fig. 10(c)). Obviously, our results are more clear and natural. Meanwhile, our results preserve the original illumination condition.

#### 4.4. Parameter selection

In this section, the effect of parameter  $\tau$  on the haze removal is analyzed to optimize the parameter setting. The parameter  $\tau$  is used to adjust distribution of luminance transmission to a similar

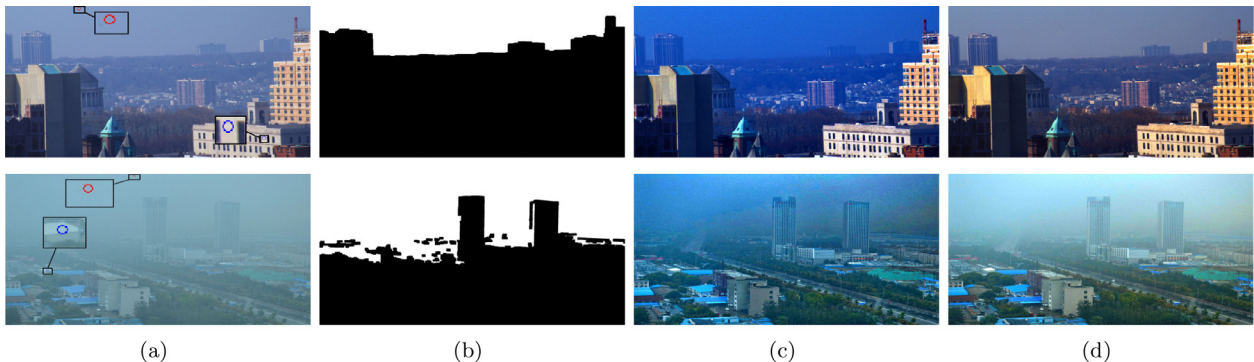


**Fig. 10.** (a) Original images. The hollow rings in the magnified area are the pixels of the atmospheric light. (b) Masks of detected sky regions. (c) Results based on original dark channel prior method. (d) Our results.

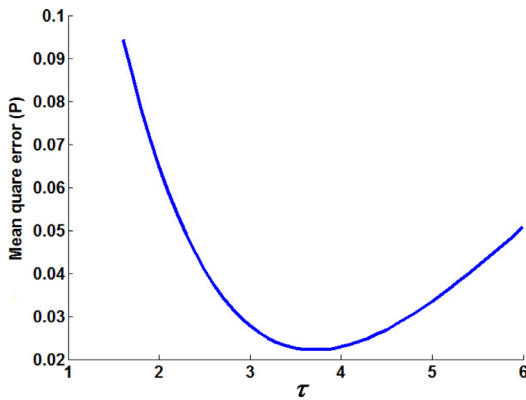


**Fig. 11.** The mean square error calculated with different  $\tau$ . 200 test images include sky in different haze concentrations are used in the mean square error calculation.

value range of dark channel prior transmission. We set the parameter  $\tau$  in different values to test the difference between dark channel prior transmission map and luminance transmission map. The difference is calculated by the following formula:

$$P(\tau) = \frac{1}{N} \sum_N (t_L(\tau) - t_d)^2 \quad (19)$$

where  $t_L$  is the transmission estimated from luminance,  $t_d$  is the transmission estimated from dark channel prior,  $N$  is the amount of test images,  $P$  is the mean square error calculated based on the setting of  $\tau$ . The relationship of mean square error  $P$  and  $\tau$  are shown in Fig. 11. The interval of  $\tau$  in 3.3–4.1 (see Fig. 11) produce the smallest difference of transmission maps (smaller than 0.024). In this value range, the luminance transmissions in most of images are closed to their dark channel prior transmissions. The higher value of  $\tau$  produces a lower value of luminance transmission and the level of haze removal will be greater. It can be used in the heavy haze weather condition. On the contrary, a low value of  $\tau$  will be more suitable for natural visual effect in the thin haze weather condition. In our experiment setting,  $\tau = 3.4$  is used for haze removal.

The transmissions of the luminance, DCP, and final fused one of two example images are shown in Fig. 12. They are aligned around the middle point of the distribution range of transmission value (see Fig. 12(d)). The dehazed results produced by our method are more natural than those produced by dark channel prior method in the sky region (compare Fig. 12(c) and Fig. 12(b)).

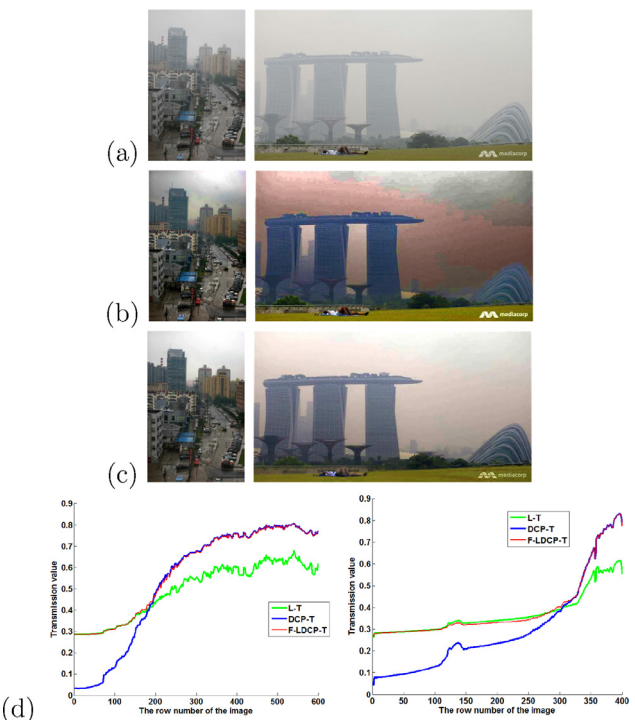


**Fig. 12.** Illustration of alignment of transmissions. (a) Input haze images. (b) Dehazed images by dark channel prior. (c) Dehazed images by our method. (d) Average transmission values in the vertical direction from sky to foreground in luminance transmission (L-T curve), dark channel prior transmission (DCP-T curve) and final transmission map (F-LDCP curve).

#### 4.5. Comparison with related methods

The proposed F-LDCP method is compared to six existing popular dehazing methods. The first method is dark channel prior [1], its results are in the second row of Fig. 13. Tarel [16] used the median filter to matting the dark channel map. Meng [18] explored the inherent boundary constraint to restore the image. Sulami's method separately derived the orientation and magnitude of atmospheric light [6]. Shi's method processed to set a threshold to divide dark channel prior transmission into the sky region and non-sky region, then it used a constant ratio to replace the sky region [3]. Cai's method was based on CNN which can generate nearly all haze-relevant features [24].

Fig. 13 shows the visual comparison of different algorithms on a few real-world examples without post-processing. The groups of images show that our algorithm handles the sky area more

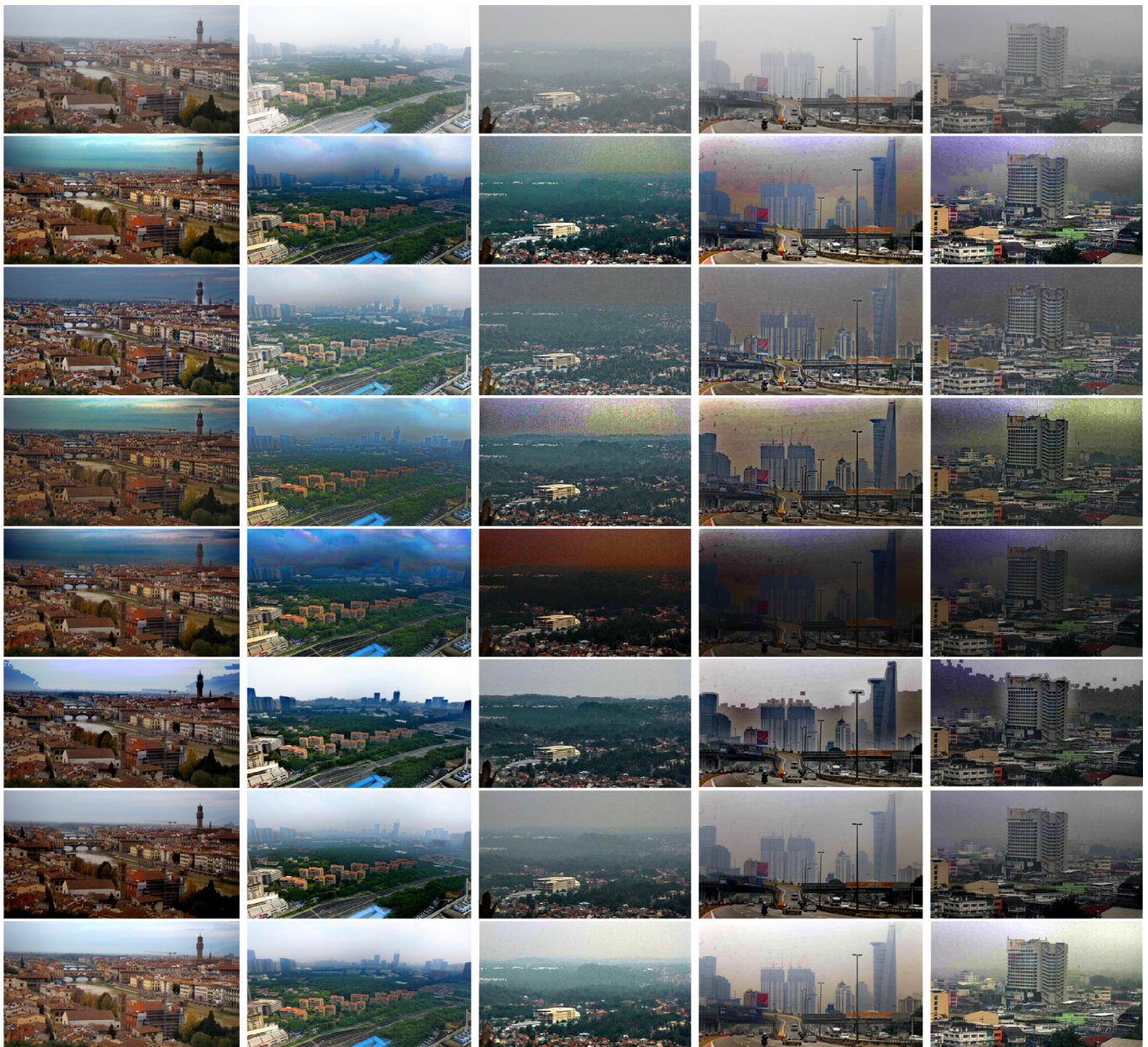


**Fig. 13.** Comparison with related methods, from top to bottom rows: original images, results by He [1], results by Tarel [16], results by Meng [18], results by Sulami [6], results by Shi [3], results by Cai [24] and our results using F-LDCP.

naturally than other algorithms. He's method produces serious distortion in the sky region. The results by Tarel and Meng looks unnatural. These two methods are not good at sky processing. Results by Sulami have weird color in sky region. Shi's results have sky details truncated as it is difficult to find an exact boundary between the sky region and non-sky region. The foreground is dark and the sky is dim in the results by Cai. Our results recover most scene details and maintain the original colors. What is more, the original image in the second column (see Fig. 13) is the UAV captured image by our own. It has no preprocessing or inhomogeneous haze. It is easy to create noises in the faraway building area after dehazing. But our method performs well without producing noise on this image.

#### 4.6. User study

To further evaluate the advantage of our method a user study was conducted. The user study was designed to evaluate

naturalness of the dehazed results. We invited 30 participants (10 females and 20 males) with ages ranging from 22 to 50. All of them have normal vision. We randomly selected 60 test images including sky region for this user study. The test image database was collected from the UAV shots, online search and the haze images in classic papers. Each original test image and its corresponding result produced by the seven methods were shown as a group. The order of the images in each group was randomly generated. The images in each group are labeled from a to h. The participants were asked to choose the one that they think was most natural.

The results of the user study are summarized in Table 1. A higher percentage of responses are in favor of our results (more than 50%). Cai's approach is also very popular (selection rate around 20%) because of its results showing the natural sky region, but the low brightness in the foreground region makes some of its results undesirable. Other methods have a low rate of selection because of the color distortion in the sky region. He's results have a clear foreground but the sky region appears dark. In addition to

**Table 1**  
User study result.

Method	He	Tarel	Meng	Sulami	Shi	Cai	Our method
Selection rate	8.94%	6.61%	3.28%	0.45%	5.78%	21.06%	<b>51.66%</b>

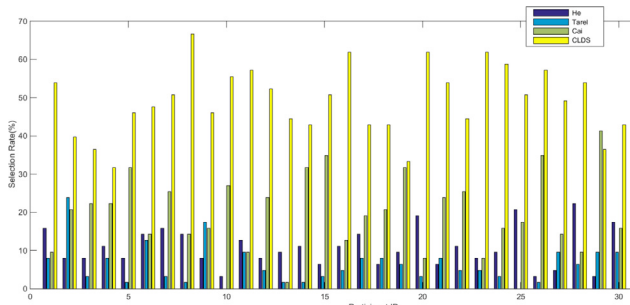


**Fig. 14.** Selection rates of the four most preferred methods He [1], Tarel [16], Cai [24], F-LDCP by the 30 participants.

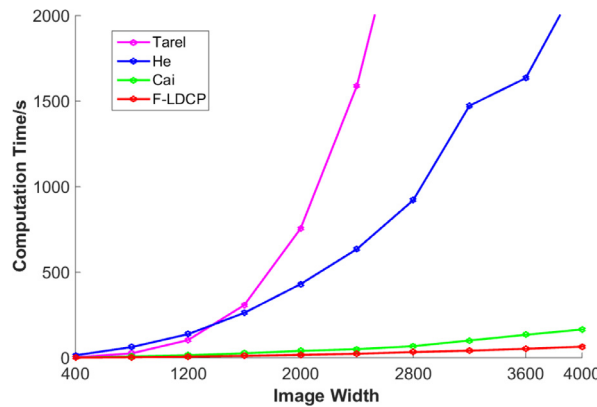


**Fig. 15.** Computational time cost of the seven methods. The images are in width/height ratio of 4/3.

the problems in the sky region, Tarel's results present halos at the corner of objects. The method by Shi is failed in the segmentation for not finding the right boundary. To analyze the coherence of the selection rates of the 30 participants, the selection rates for the top four preferred methods by the 30 participants are plotted in Fig. 14. Our method is uniformly preferred by all the participants (our method takes the maximum selection rate). However, there are participants whose selection rate of our method is less than 45%. According to the feedback of these participants, some of our results are over-enhanced.

#### 4.7. Time cost

The computational time costs of the seven methods are plotted in Fig. 15. He's and Tarel's methods could only be run on the PC with 8G or above memory because of high memory usage when processing images with a resolution of  $4000 \times 3000$ . Therefore, the experiments were implemented with Matlab R2014a on a PC with a 2.60 GHz Intel Xeon E5-2690 v3 CPU and 256 GB of HD. Ten UAV images were resized to different resolutions and used for the computational time calculations. According to Fig. 15, our method is the fastest for processing a UAV image, because the Fast Guided Filter [9] is faster than Laplacian matrix which is used in [8], to refine the rough transmission estimated by the dark channel prior method. The running time of the fast guided filter is about 4s for a  $4000 \times 3000$  image, in contrast to 1490 s using the matting Laplacian matrix [8]. Others cost of estimation in the dark channel map

**Table 2**  
Objective assessment result.

	PSNR	SSIM	e	$\bar{r}$	$\Sigma$
He	18.33	0.73	1.99	2.25	$1.80 \times 10^{-3}$
Tarel	18.31	0.76	1.57	<b>2.42</b>	$2.64 \times 10^{-6}$
Meng	17.06	0.74	1.50	2.24	$1.15 \times 10^{-4}$
Sulami	14.02	0.60	<b>2.06</b>	1.80	$5.60 \times 10^{-3}$
Shi	17.26	0.72	1.81	1.93	$2.56 \times 10^{-2}$
Cai	21.31	0.75	0.95	1.54	$5.11 \times 10^{-2}$
F-LDCP	<b>21.53</b>	<b>0.78</b>	1.16	1.90	<b><math>1.26 \times 10^{-6}</math></b>

is about 40 s and the airlight value is about 10 s. The total cost of an UAV image in resolution of  $4000 \times 3000$  using our F-LDCP method is about 54 s.

#### 4.8. Objective assessment

Besides the user study, we also analyzed five quantitative evaluation metrics to assess our proposed algorithm. As it was difficult to acquire the corresponding ground truth data for the input haze images, we proposed to add haze for haze-free images with depth to generate haze images for performing our objective assessment. 100 outdoor images with depth were collected from the Make3D project [30,31]. Haze was added in these images based on the real depth to generate haze images. Our method was used to remove the haze in these haze images. The original haze-free images served as the ground truth for comparison with our dehaze results.

PSNR (Peak Signal to Noise Ratio) and SSIM (Structural Similarity Index) [32] were the two criteria to evaluate the differences between each pair of ground truth haze-free image and dehazed result. Other three evaluation metrics measured by using the haze image as the reference were: the rate of visible edges numbers e, the average visibility enhancement obtained by the restoration algorithm  $\bar{r}$ , and the percentage of pixels  $\Sigma$  was completely black or completely white after restoration [33]. The objective assessment result are summarized in Table 2. Our PSNR value and SSIM value are the highest. It confirms that our result is the closest to the ground truth. However, the e and  $\bar{r}$  values of our method are low. This is because our method does not produce over sharpened edges. He's and Meng's results have a large amount of noise in the sky region, Tarel's results have clear halos around edges and corners, and Shi's results have a clear boundary between sky region and other regions. They are the reason for the large value of visible edge detection e. The ratio of black or white pixels  $\Sigma$  in our results is the lowest due to correct airlight estimation, which keeps the whole image away from dim and excessive exposure.

The dehazed results of an image are compared to the ground truth in Fig. 16. we can see that our result retains the best natural weather condition in sky region, which is similar with the ground truth. Cai's [24] PSNR score is close to us, but Cai's result usually gets a little hazy and the foreground is too dim. Their  $\Sigma$  score illustrates that their results have a lot of black points. The results of He [1], Tarel [16], Meng [18], Sulami [6] and Shi [3] have large e and  $\bar{r}$  values than our method. This is because results of these methods have a large amount of noise in the sky region. Our method does not produce over sharpened edges.

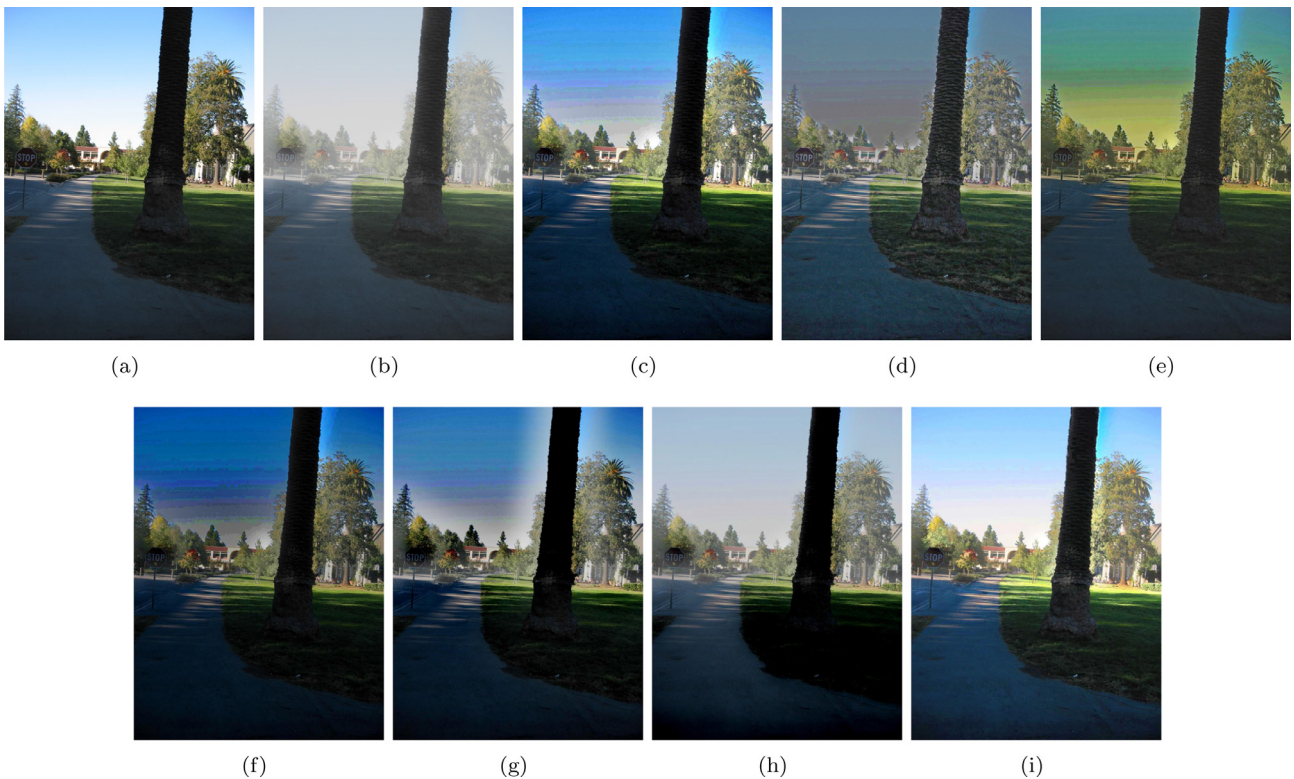


**Fig. 16.** The comparison of results to ground truth.



**Fig. 17.** Dehazed result of an image without sky. (a) Input image. (b) Our result.

#### 4.9. Dehazing non-sky images

While our method performs well for images with sky, it can also be used for images without sky. The edge detection step in atmospheric estimation can classify the image to be with or without sky. For images without sky, the initial transmission map will be obtained by dark channel prior method [1], and further refined using fast guided filter [9]. An example dehazed results of an image without sky is shown in Fig. 17.

#### 5. Limitation

The atmospheric estimation only selects the median value of the 1% brightest pixel values in the sky region. It is not stable for picking out a pixel value as the atmospheric airlight. When airlight is picked in the sun region, the image will color shift. We have tried to use the mean value of the 1% brightest pixel values in the sky region, but it is hard to avoid color shift in whole image. In the future, we will try to estimate atmospheric airlight in local patches. On the other hand, even though the processing speed is improved in our method, it takes approximately 54 s to process a UAV image with a resolution of  $4000 \times 3000$ . The main cost is from dark channel computation and atmospheric airlight estimation. In

the future, we will develop a method to achieve real-time speed for UAV images.

#### 6. Conclusion

In this paper, we have proposed a simple but ingenious and good-effective method for single image haze removal. We analyzed the main problems of dark channel prior method and proposed a novel model to solve them in dehazing of images with sky. We referred to our method as the F-LDCP method. The method is effective for processing long shot scene, in removing haze without color shift and retaining the visual truth. The proposed method has been tested in the UAV images with high resolution, and the result is effective within acceptable computational time. The comparison of our method with related state-of-the-art methods has demonstrated the advantages of our method in preserving naturalness of images with sky.

#### Acknowledgment

This work was supported in part by: (i) the National Natural Science Foundation of China (Grant No. 61602314, 61602313, 61620106008, and 61602312); (ii) the Natural Science Foundation of Guangdong Province of China (Grant No. 2016A030313043); (iii) Fundamental Research Project in the Science and Technology Plan of Shenzhen (Grant No. JCYJ20150324141711630, JCYJ20130326105637578, JCYJ20170302153632883, JCYJ20160226191842793, and JCYJ2016033114551175); (iv) Tencent “Rhinoceros Birds” - Scientific Research Foundation for Young Teachers of Shenzhen University; (v) Shenzhen University research funding (2016051).

#### References

- [1] K. He, J. Sun, X. Tang, Single image haze removal using dark channel prior, *IEEE Trans. Pattern Anal. Mach. Intell.* 33 (12) (2011) 2341–2353.

- [2] G. Wang, G. Ren, L. Jiang, T. Quan, Single image dehazing algorithm based on sky region segmentation, *Inf. Technol. J.* 12 (6) (2013) 1168–1175.
- [3] Z. Shi, J. Long, W. Tang, C. Zhang, Single image dehazing in inhomogeneous atmosphere, *Optik - Int. J. Light Electron Opt.* 125 (15) (2014) 3868–3875.
- [4] F. Yu, C. Qing, X. Xu, B. Cai, Image and video dehazing using view-based cluster segmentation, in: *Visual Communications and Image Processing (VCIP)*, 2016, IEEE, 2016, pp. 1–4.
- [5] I. Yoon, S. Jeong, J. Jeong, D. Seo, J. Paik, Wavelength-adaptive dehazing using histogram merging-based classification for uav images, *Sensors* 15 (3) (2015) 6633–6651.
- [6] M. Sulami, I. Glatzer, R. Fattal, M. Werman, Automatic recovery of the atmospheric light in hazy images, in: *IEEE International Conference on Computational Photography (ICCP)*, 2014, IEEE, 2014, pp. 1–11.
- [7] K. Tang, J. Yang, J. Wang, Investigating haze-relevant features in a learning framework for image dehazing, in: *2014 IEEE Conference on Computer Vision and Pattern Recognition*, IEEE, 2014, pp. 2995–3002.
- [8] A. Levin, D. Lischinski, Y. Weiss, A closed form solution to natural image matting, *IEEE Trans. Pattern Anal. Mach. Intell.* 30 (2) (2008) 228–242.
- [9] K. He, J. Sun, Fast guided filter, *Comput. Sci.* (2015). arXiv preprint arXiv:1505.00996.
- [10] K. He, J. Sun, X. Tang, Guided image filtering, *IEEE Trans. Softw. Eng.* 35 (6) (2013) 1397–1409.
- [11] S.K. Nayar, S.G. Narasimhan, Vision in bad weather, in: *IEEE International Conference on Computer Vision*, 1999, pp. 820–827. vol.2
- [12] S.G. Narasimhan, S.K. Nayar, Contrast restoration of weather degraded images, *IEEE Trans. Pattern Anal. Mach. Intell.* 25 (6) (2003) 713–724.
- [13] R.T. Tan, Visibility in bad weather from a single image, in: *IEEE Conference on Computer Vision and Pattern Recognition, 2008 CVPR 2008.*, IEEE, 2008, pp. 1–8.
- [14] R. Fattal, Single image dehazing, *AcM Trans. Graph.* 27 (3) (2008) 1–9.
- [15] J. Kopf, B. Neubert, B. Chen, M. Cohen, D. Cohen-Or, O. Deussen, M. Uyttendaele, D. Lischinski, Deep photo: model-based photograph enhancement and viewing, *AcM Trans. Graph.* 27 (5) (2008) 32–39.
- [16] J.P. Tarel, N. Hautiere, Fast visibility restoration from a single color or gray level image, in: *IEEE International Conference on Computer Vision*, 2009, pp. 2201–2208.
- [17] K. Nishino, L. Kratz, S. Lombardi, Bayesian defogging, *Int. J. Comput. Vis.* 98 (3) (2011) 263–278.
- [18] G. Meng, Y. Wang, J. Duan, S. Xiang, C. Pan, Efficient image dehazing with boundary constraint and contextual regularization, in: *Proceedings of the IEEE International Conference on Computer Vision*, 2013, pp. 617–624.
- [19] Y. Li, Q. Miao, J. Song, Y. Quan, W. Li, Single image haze removal based on haze physical characteristics and adaptive sky region detection, *Neurocomputing* 182 (2016) 221–234.
- [20] B. Cai, X. Xu, D. Tao, Real-time video dehazing based on spatio-temporal mrf, in: *Pacific Rim Conference on Multimedia*, Springer, 2016, pp. 315–325.
- [21] Q. Zhu, J. Mai, L. Shao, A fast single image haze removal algorithm using color attenuation prior, *IEEE Trans. Image Process.* 24 (11) (2015) 3522–3533.
- [22] T. Bui, H. Tran, W. Kim, S. Kim, Segmenting dark channel prior in single image dehazing, *Electron. Lett.* 50 (7) (2014) 516–518.
- [23] W. Ren, S. Liu, H. Zhang, J. Pan, X. Cao, M.-H. Yang, Single image dehazing via multi-scale convolutional neural networks, in: *European Conference on Computer Vision*, Springer, 2016, pp. 154–169.
- [24] B. Cai, X. Xu, K. Jia, C. Qing, D. Tao, Dehazenet: An end-to-end system for single image haze removal, *IEEE Trans. Image Process.* 25 (11) (2016) 5187–5198.
- [25] E.J. McCartney, *Optics of the atmosphere: scattering by molecules and particles*, John Wiley and Sons, Inc., New York, 1976, p. 421.
- [26] A.J. Preetham, P. Shirley, B. Smits, A practical analytic model for daylight, in: *Proceedings of the 26th Annual Conference on Computer Graphics and Interactive Techniques*, ACM Press/Addison-Wesley Publishing Co., 1999, pp. 91–100.
- [27] S.G. Narasimhan, S.K. Nayar, Shedding light on the weather, in: *Proceedings. 2003 IEEE Computer Society Conference on Computer Vision and Pattern Recognition*, 2003, 1, IEEE, 2003, 1–1.
- [28] J. Chen, T.N. Pappas, A. Mojsilovic, B.E. Rogowitz, Adaptive perceptual color-texture image segmentation, *IEEE Trans. Image Process.* 14 (10) (2005) 1524–1536.
- [29] S. Anand, S. Mittal, O. Tuzel, P. Meer, Semi-supervised kernel mean shift clustering, *IEEE Trans. Pattern Anal. Mach. Intell.* 36 (6) (2014) 1201–1215.
- [30] A. Saxena, S.H. Chung, A.Y. Ng, Learning depth from single monocular images, in: *Advances in Neural Information Processing Systems (NIPS)*, 2006, pp. 1161–1168.
- [31] A. Saxena, S.H. Chung, A.Y. Ng, 3-d depth reconstruction from a single still image, *Int. J. Comput. Vis.* 76 (1) (2008) 53–69.
- [32] Z. Wang, A.C. Bovik, H.R. Sheikh, E.P. Simoncelli, Image quality assessment: from error visibility to structural similarity, *IEEE Trans. Image Process.* 13 (4) (2004) 600–612.
- [33] N. Hautire, J.P. Tarel, D. Aubert, DUMONT, blind contrast enhancement assessment by gradient ratioing at visible edges, *Image Anal. Stereol.* 27 (2) (2008) 87–95.



**Yingying Zhu** received the B.S. degree in computer science from Wuhan University, China, in 1998, and the M.S. degree in computer science from Wuhan University, in 2001, and her Ph.D. degree in computer science from Wuhan University, in 2004. She is currently an associate professor in the college of Computer Science and Software Engineering, Shenzhen University, China. She is also a member of China Computer Federation. Her research interests include multimedia content analysis, information retrieval and multimedia information security.



**Gaoyang Tang** received this B.S. degree from the School of Beijing Institute of Technology, Zhuhai, China in 2015. She is currently working toward the M.S. degree in the Department of software engineering, College of Computer Science and Software Engineering, Shenzhen University, Shenzhen, China. Her current research interests include digital image processing and deep learning.



**Xiaoyan Zhang** received the Ph.D. degrees from School of Electrical and Electronic Engineering, Nanyang Technological University, Singapore, in 2014. She was a research fellow in Houston Methodist Research Institute, Houston, US, from 2013 to 2015. She is currently a lecturer in College of Computer Science & Software Engineering, Shenzhen University, China. Her current research interests include 2D image rendering, medical image processing, and 3D object modeling.



**Jianmin Jiang** received Ph.D. from the University of Nottingham, UK, in 1994. From 1997 to 2001, he worked as a full professor of Computing at the University of Glamorgan, Wales, UK. In 2002, he joined the University of Bradford, UK, as a Chair Professor of Digital Media, and Director of Digital Media & Systems Research Institute. He worked at the University of Surrey, UK, as a full professor during 2010–2015 and a distinguished professor (1000-plan) at Tianjin University, China, during 2010–2013. He is currently a Distinguished Professor and director of the Research Institute for Future Media Computing at the College of Computer Science & Software Engineering, Shenzhen University, China. He was a chartered engineer, fellow of IEE, fellow of RSA, member of EPSRC College in the UK, and EU FP-6/7 evaluator. His research interests include, image/video processing in compressed domain, digital video coding, stereo image coding, medical imaging, computer graphics, machine learning and AI applications in digital media processing, retrieval and analysis. He has published around 400 refereed research papers.



**Qi Tian** received his Ph.D. in ECE from University of Illinois at Urbana-Champaign (UIUC) in 2002 and received his B.E. in Electronic Engineering from Tsinghua University in 1992 and M.S. in ECE from Drexel University in 1996, respectively. Qi Tian is currently a Full Professor in the Department of Computer Science, the University of Texas at San Antonio (UTSA). He was a tenured Associate Professor from 2008–2012 and a tenure-track Assistant Professor from 2002–2008. Dr. Tian's research interests include multimedia information retrieval, computer vision, pattern recognition and bioinformatics.